Celal Bayar University Journal of Science

Empirical Advancements in Field Oriented Control for Enhanced Induction Motor Performance in Electric Vehicle

Mussaab Alshbib[1], Sohayb Abdulkerim[2]*

[1]Sham University, Ezaz, Syria
[2] Department of Aerospace Engineering, Gaziantep University, 27310, Gaziantep, Türkiye

*karim@gantep.edu.tr,
*Orcid No: 0000-0002-3448-9129

Received: 15 March 2024
Accepted: 31 August 2024
DOI: 10.18466/cbayarfbe.1453798

Abstract

This paper introduces an advanced Field Oriented Control (FOC) strategy, specifically tailored for electric vehicle drivetrains, that streamlines the tuning process of PI controllers within the α and β coordinates of the synchronous reference frame. The innovative approach mitigates torque and stator current fluctuations while maintaining a constant switching frequency and improves inverter voltage use through third harmonic injection. Crucially, the theoretical underpinnings and simulation outcomes, obtained via MATLAB/Simulink, are substantiated by rigorous experimental verification. A dedicated DS1103-controlled testbed replicates real-world electric vehicle conditions, demonstrating the practical efficacy of the FOC method. The experimental results underscore the robustness of the control strategy across a broad range of operating scenarios, establishing a significant leap forward in electric vehicle control technology.

Keywords: Voltage Source Inverter; Induction Motor, Electric Vehicles, Control Nonlinearities, Control System Synthesis

1. Introduction:

Several types of electric motors are widely used for EVs, including DC-brushed motors, DC brushless motors, permanent magnet synchronous motors (PMSMs), induction motors (IMs), and switch-reluctant motors (SRMs). The induction motors are the most commonly used in industry and traction applications since they are of good construction, lower cost, ease of fault detection, and lower power to weight ratio when compared with the permanent magnet synchronous motors [1]. In various industrial applications, such as robotics, heavy industry, ships, and renewable energy systems, there are two methods known to researchers: Field Oriented control (FOC) [2]-[3], and direct torque and stator flux control (DTC) [4]-[5].

Although the requirements for implementing the FOC strategy are more complex than the DTC strategy, especially the need to estimate or measure speed, it is more widespread and reliable, especially in electric vehicle applications.[6]. Therefore, the efforts of researchers focused on developing this strategy by introducing modern technologies that achieve high reliability while maintaining strong performance at the same time. The implementation of the FOC strategy using PID regulators has been widespread in many applications of FOC, such as driving a BLDC Motor enhanced by parallel optimized technique [7]. In the research [8], a PI regulator was used in the speed control loop of an induction motor with the use of a genetic algorithm to estimate the regulator values. However, this research lacked practical implementation that supported theoretical analysis. DSP based-Fuzzy FOC control method of permanent magnet synchronous motor was performed in [9]. The authors tried to simplify the design of the algorithm by using the toolbox in Matlab. However, they set manual values for parameters in addition to not testing the designed system on a wide range of operating conditions. A similar work to Research [9] was proposed in the paper [10] where the FOC strategy was applied to an induction motor with PI parameter values adjusted with the help of the Fuzzy controller. The speed signal was also obtained from Lunberger's estimator. However, this research was limited to theoretical simulation without practical application.

A modified research proposed by the researchers in [11] by applying the strategy to brushless DC motor with enhanced fuzzy controller. The authors tested their approch in cases of no load and load with variable speed. As it is known, the windup phenomenon is a negative one caused by PI controllers. This phenomenon has been analyzed in [12], which presented a study of solutions of antiwindup techniques to reduce problem of saturation suffered by these controllers in PMSM engines. The most advanced techniques have been introduced into the algorithm such as the use of neural networks as in [13].

The rest of this article is arranged as follows. Section 2 presents a detailed background for the FOC strategy. Section 3 presentes formulation FOC strategy of IM. Simulation and experimental results are outlined in Section 3 and Section 4 to verify the feasibility and effectiveness of the proposed strategy. Finally, the conclusion is performed in Section 5.

2. Theoritcal Background of FOC Algortihm

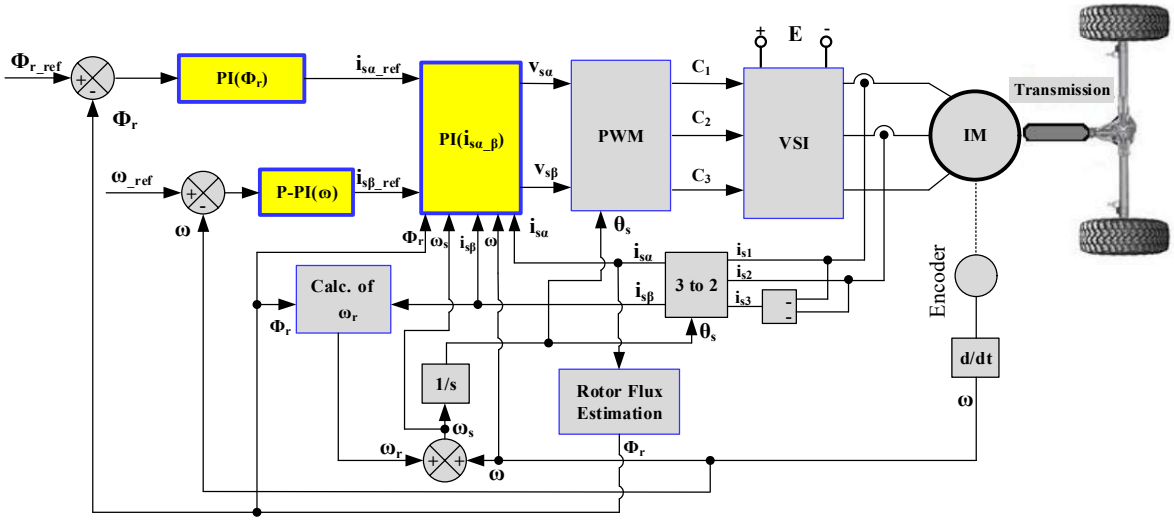

Figure 1. The block diagram of FOC of IM

where the researchers replaced the PID controller in the current loop with a neural network while maintaining the PID regulators in the speed loop. The work is especially noteworthy since it was tested in the field weakining region of PMSM motor, yet it was not without difficulty in tuning and training the network.

Model Predictive Contorl (MPC) principles based PID-FOC techniques to improve the performance in propulsion systems [14], MPC based FOC of the induction motors in electric vehicles [15], or MPC based FOC of five phase PMSM are are some of the research published within this context. In [16], The inverter investment in FOC algorithm was enhanced sliding mode and the injection of the third harmonic component. This proposed method was applied in an [16]- asynchronous generator of single-rotor wind turbine. These techniques have been used in other research in order to suppress the current harmonics [17], and to reduce the oscillations of both torque and magnetic flux [18].

This paper proposes an effective and simple method of field oriented control FOC which is suitable electric vehicles applications. The proposed scheme ensures the low chattering of the torque and the stator currents with fixed frequency. In addition, It is enhanced by using the third harmonic injection technique which improves the utiliy of the inverter voltage.

In fact, the orientation of the field control algorithm varies according to the method of obtaining the orientation angle. The name of direct field orientation (DFOC) control algorithm is given to that algorithm in which the value of the orientation angle is obtained from the direct measurement of the magnetic flux. This method is limited in use due to the difficulty of measuring the magnetic flux (for the stator or the rotor) directly, and it is also costly due to the need for a magnetic flux sensor. In contrast, the Indirect Field Orientation Control (IFOC) algorithm is defined as the algorithm that uses a slip relationship, that is, by adding the speed of the rotor ω with the slip speed ω_r [19]. Due to its dependence on the sliding relationship, it is influenced by machine parameters, yet it is considered the primary method used to flux orientation control of induction motors. Note that in both methods (direct and indirect flux orientation control), the presence of the current control loop stage is preferred. Therefore, Hystereis regulators can be used at this stage or any type of traditional or smart regulator [20].

The detailed block scheme of the direct FOC strategy is shown in Figure (1). It has two loops of control, the first loop is to control the modulus of the rotor flux, while the second one is to control the rotor speed [21]. The three phase currents of the motor are captured, which are used to obtain two phases currents in synchronous reference

Celal Bayar University Journal of Science
Volume 20, Issue 3, 2024, p 47-57
Doi: 10.18466/cbayarfbe.1453798

frame. The orientation angle is calculated depending on the rotor speed calculated from the position of the motor shaft, and load-dependent slip speed. The two phases voltages are introduced within the PWM stage in order to obtain the suitable pulses to be applied to the electronic switches of the mold driving the motor [22].

3. FOC strategy formulation

In the FOC strategy, control is achieved through two separate loops: the rotor flux control loop along the α-axis and the speed control loop along the β-axis. Figure (2) illustrates the block diagram for this structure, detailing the rotor flux control for the α-axis Figure (2a) and the speed control for the β-axis Figure (2b).

The mathematical model in terms of the stator currents of the rotor flux is given as follows [23] [24]:

$$\begin{bmatrix} \frac{d\underline{i}_s^k}{dt} \\ \frac{d\underline{\Phi}_r^k}{dt} \end{bmatrix} = \begin{bmatrix} \frac{1}{\sigma L_s} \\ 0 \end{bmatrix} \underline{V}_s^k + \begin{bmatrix} -\frac{1}{\sigma\tau_s} - \frac{L_m^2}{\sigma\tau_r L_s L_r} - j\omega_k & \frac{L_m}{\sigma L_s L_r}\left(\frac{1}{\tau_r} - j\omega\right) \\ \frac{L_m}{\tau_r} & -\frac{1}{\tau_r} - j(\omega_k - \omega) \end{bmatrix} \begin{bmatrix} \underline{i}_s^k \\ \underline{\Phi}_r^k \end{bmatrix} \quad (1)$$

Where, $\underline{V}_s^k$ is the stator voltage vector; L_s, L_r, and L_m are the stator, rotor, and mutual self inductances respectively; $(\sigma = 1 - \frac{L_m^2}{L_S L_r})$ is the leakage constant; τ_s, τ_r refer to the time constant of the stotor rotor respectively,

$$\frac{d\Phi_{s\alpha}^s}{dt} = V_{s\alpha}^s - R_s i_{s\alpha}^s \quad (2)$$

$$\frac{d\Phi_{s\beta}^s}{dt} = V_{s\beta}^s - R_s i_{s\beta}^s \quad (3)$$

$$\Phi_{r\alpha} = \frac{a_2}{s + a_1} i_{s\alpha} \quad (4)$$

where, R_s is the stator resistance for one phase.

The real rotor flux component, taking into account the the rotor flux vector orientation, can be written as [25]:

The slip frequency ω_r is calculated by one of the two equations [26]:

$$\omega_r = \frac{a_2 i_{s\beta}}{|\Phi_r|} \quad (5)$$

$$\omega_r = \frac{a_2}{\Phi_r}\frac{L_r}{pL_m}\frac{T_{em}}{\Phi_r} = \frac{a_2 L_r}{pL_m \Phi_r^2} T_{em} \quad (6)$$

the motor torque can be written as follows, via substituting the formula (5) into the formula (6),

$$T_{em} = \frac{pL_m}{L_r}(\Phi_r i_{s\beta}) \quad (7)$$

The angle of orientation can be estimated using the equation [27]:

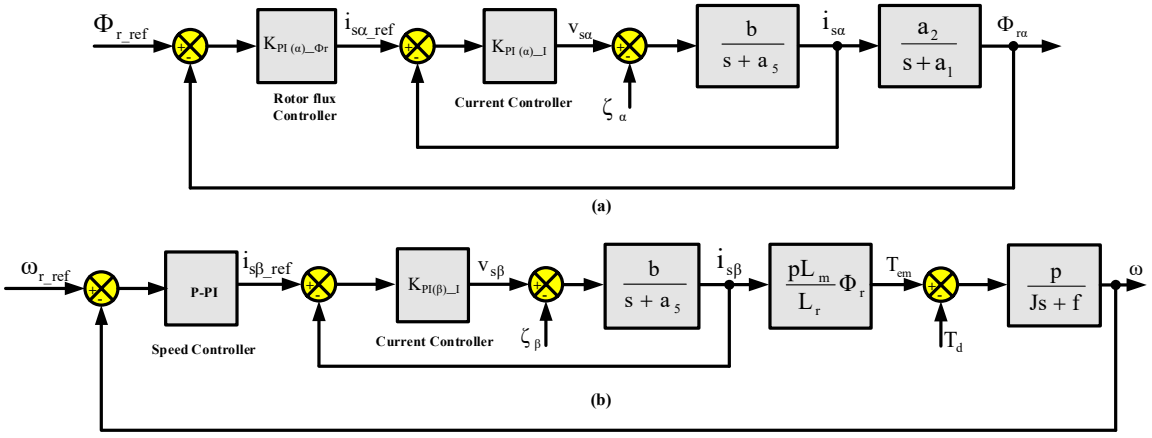

Figure 2. Clarifies the block diagram of both the rotor flux control and the speed control of FOC strategy of α-axis, and β-axis, respectively, (a) Rotor flux control for α-axis, (b) Speed control for β-axis.

ω is the rotational speed; p is the pole pairs number

the components of the stator flux vector are given as follows,

$$\omega_s = \omega_r + \omega \quad (8)$$

In order to accomplish the control process, PI regulators will be used for thoughtful control loops. This choice is due to the simplicity of these controllers compared to

Celal Bayar University Journal of Science
Volume 20, Issue 3, 2024, p 47-57
Doi: 10.18466/cbayarfbe.1453798

other controllers, and their ability to cancel the steady state error [28]. However, They suffer from instability due to the fact that they contain the integrator. Therefor, this problem will be solved by using antiwindup technique that eliminates the malfunction condition of the regulator's operation [29]. Due to its simplicity as well as its ability in maintaining the system order, the technique of zero-pole cancellation will be used for calculating the gains of the controllers [30].
The controller rotor flux as well as the speed regulator gains are calculated after calculating the current controller gains in the inner loop.The detailed calculations is performed in the Appendix A.

4. Simulation Results

The tested motor was an induction motor of squirrel cage type. Its nominal speed at *282.7 [rad/sec]*, The nominal torque and the rotor flux are *0.945[Wb]*, *1.76 [Nm]*, respectively. Its nominal power was *0.25[Kw]*. In order to investigate the the FOC performance, important parameteres should be set as follows. The inverter switching frequency and the sampling period were set as f_{PWM}=10[KHZ] and T_s=50[µs], respectively. The technique of the third harmonic injection was used in order to enhance the reference voltages with PWM stage (That means an increasing of 15.47% of ($\frac{E}{\sqrt{2}}$) is gained) [31].

In order to test the performance of the proposed method over a wide speed range, the simulation results are conducted in Figure (3). Consecutive jumps in the reference speed signal with different values made at specific times. At the moment 0.3 seconds, a reference speed of 100 [rad/sec] was requested. At the moment 3, a reference speed of 150 [rad/sec] was requested. At moment 5 seconds, A negative reference speed of -50 [rad/sec] was requested until the moment 7.5 seconds a positive reference speed requested again. It is observed that the measured speed of the motor was well tracked the reference speed without any disturbances in transient states. The developed torque of the motor followed the changes of the speed with low chattering and high dynamics. The rotor flux was maintained controlled around its nominal value (0.945 [Wb]). The motor three currents remained sinusoidal without spikes during transitions changes.

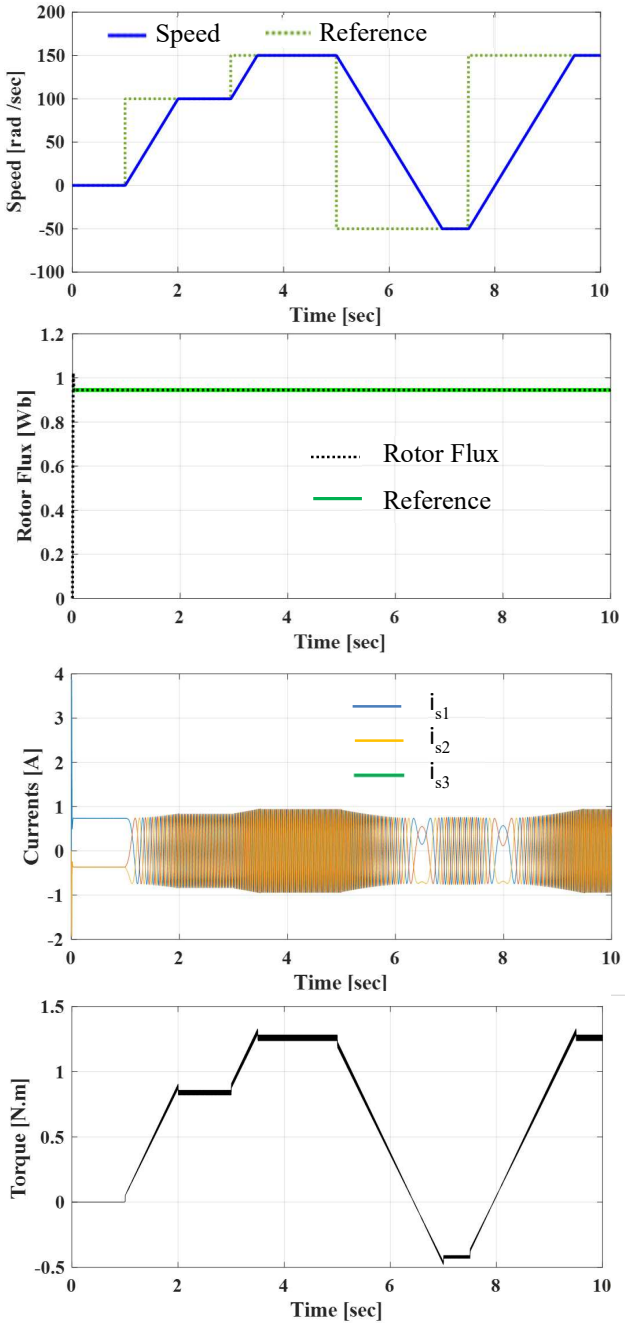

Figure 3. Behaviour of FOC strategy for wide speed range.

To verify the correct α-axis orientation in terms of the rotor flux vector since it is the core of FOC strategy, the two components of Φ_r vector were plotted, for the the frame (α, β), in Figure (4). it is indeed observed that the imaginary component is approximately equalled zero, and the real component is approximately equalled the value of the nominal rotor flux magnitude as it reached the value 0.951[wb].

Celal Bayar University Journal of Science
Volume 20, Issue 3, 2024, p 47-57
Doi: 10.18466/cbayarfbe.1453798

00000000

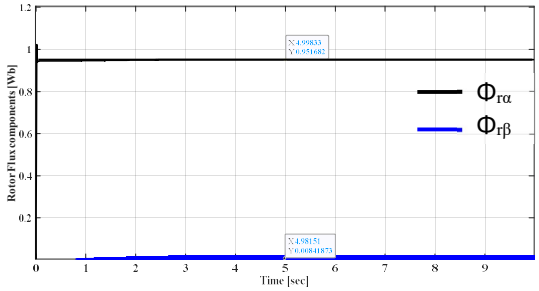

Figure 4. Components responses of the rotor flux vector

Similarly, Figure (5) shows the components of the stator current vector for the synchronous frame. It is noted that the current of α- axis reached 4.75A during the startup, while it stabilized in the steady state at 0.89A. On the other hand, the imaginary current increased gradually due to the graded reference speed and stabilized at a value of 1.32A.

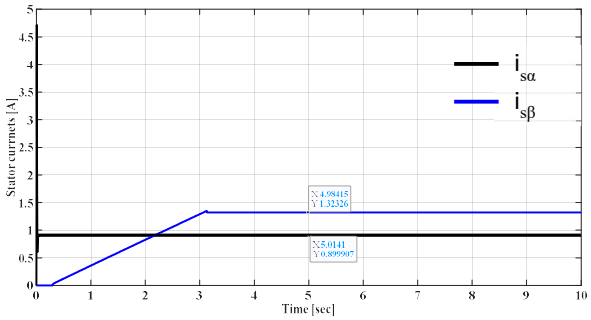

Figure 5. The two components of the stator current vector

Figure (6) clarifies the three-phase voltage signals before being injected with the third harmonic signal divided by the parameter (E) with the third harmonic signal. With this case, an extra reference voltages could be secured by an increase of (15.47%), or the DC-link could be reduced by 15.47%.

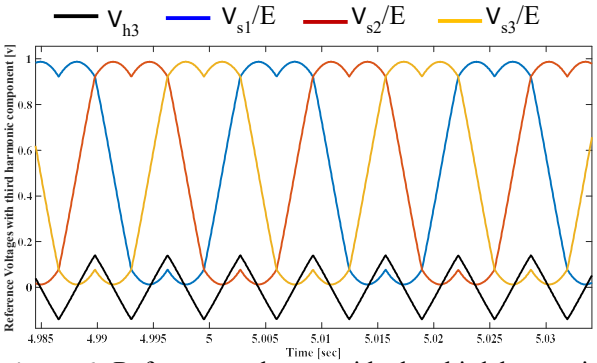

Figure 6. Reference voltages with the third harmonic injection technique

Figure (7) shows the voltage vector amplitude developed from the FOC algorithm. The nominal voltage of the tested motor is 230V, that is, the maximum value of the nominal voltage is 325V. Since the two phases voltages amplitude is greater than the three phases voltages by 1.224, the maximum value of the Vs in the synchronous frame is 400V. However, there is an increase in this value of 24[V]. This increase is due to the optional gains. These values can be changed to obtain less voltage, but this change may cause worse performance of the system, so a slight overrun of the applied voltage to the motor can be accepted.

Figure (8) shows the slip speed with the orientation angle in the synchronous reference frame.

The slip speed has a similar response to the torque response according to equation (6) for a constant rotor flux value.

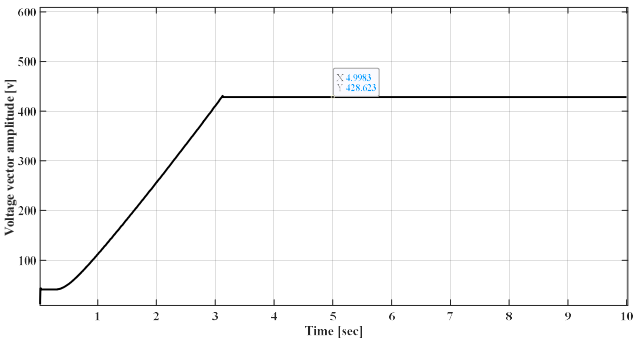

Figure 7. Voltage vector amplitude response

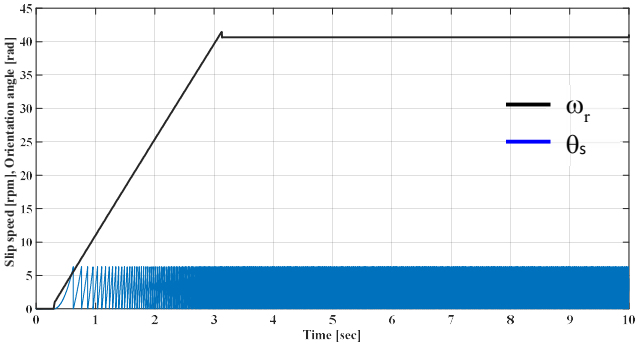

Figure 8. Slip speed and orientation angle responses

5. Experimental results

In order to test the performance of the approach over a wide range of speed and verify the the simulation results, experiments were carried out on a test rig within the laboratory equipped for electric drive systems. The platform has been invested in some of our literature research [32]. The experiments were conducted on a 50Hz, 230/400V squirrel cage three-phase induction motor with a power of 0.25 kW, a rated speed of 1350 rpm, and a rated torque of 1.76 Nm. Full details of the motor's parameters are provided in Appendix B. The motor was powered by a 22.8 kVA three-phase Semikron inverter, with the DC-link voltage set at 550V.

The core component of the platform is the DS1103 digital processing card which is supported by dSPACE company. The card is supported by a graphical environment (called ControlDesk) that helps the designer to build a control interface that is used for the control commands and monitoring measured and calculated signals in real time. As for the sensors in the platform, they are two current-sensors, a differential sensor to measure the inverter dc-link. The interface circuit for the current sensors outputs ±0.5V for each ±1A of input. The currents were fed into three channels of the 4-channel Analog-Digital Converter (DS1103ADC_Cx). This ADC divides its input by 10, so an input range of [-10, +10] yields an output range of [-1, +1]. To get the actual current value, the output signal of the ADC must be multiplied by a gain factor of 20 (2 × 10). In addition, An incremental encoder with 1024 pulses per revolution was used to measure speed. The conversion between mechanical speed and electrical speed is achieved by multiplying by the number of pole pairs. To calculate the position differential, the current position is subtracted from the previous position, and then the result is multiplied by the conversion factor to obtain the electric speed. First-order intermediate filters were used to minimize noise during position signal acquisition from the encoder.

The interface circuit for the measured DC-link outputs ±0.5V for every ±100V of input. This ADC_20 divides its input by 10. To get the actual DC-link voltage, the output signal from the ADC_20 must be multiplied by a gain of 2000 (200 × 10).
As for the inverter, it is a three-phase of Semikron type that has the capabilities of adding dead time to the driving transistors in addition to its capabilities in protecting the motor and dSPACE at any sudden error or failure. The block diagram of the platform and the experimental setup is shown in Figure (9) and Figure (10), resecitvely.

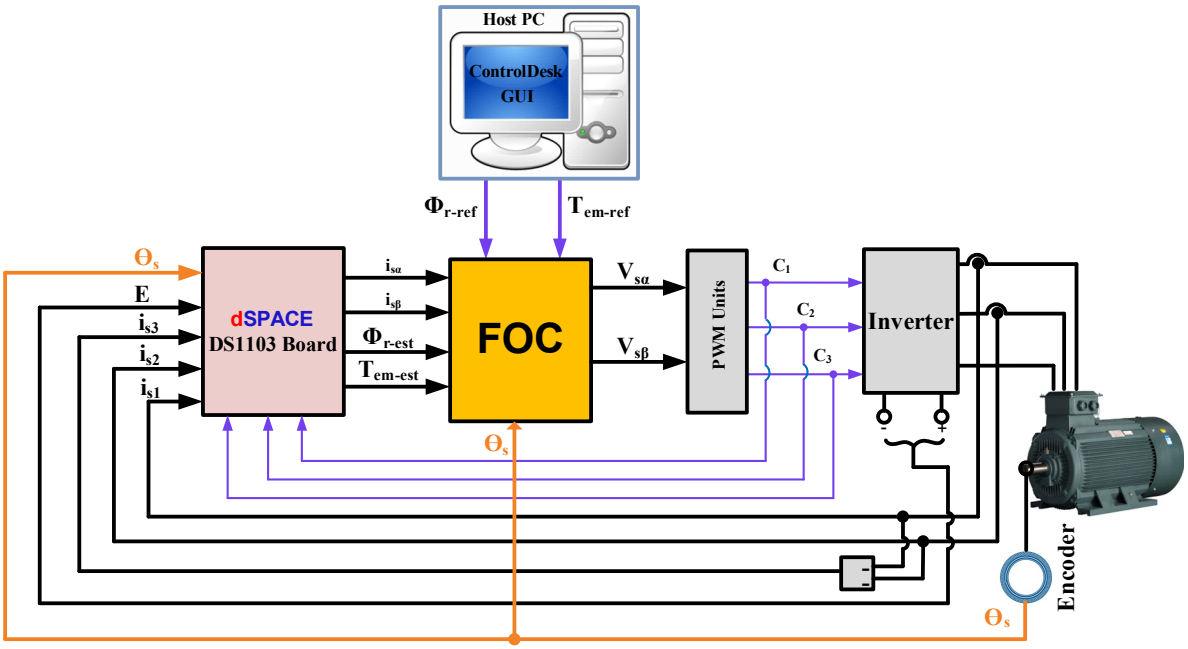

Figure 9. Block diagram of the test rig for experimental test of FOC method

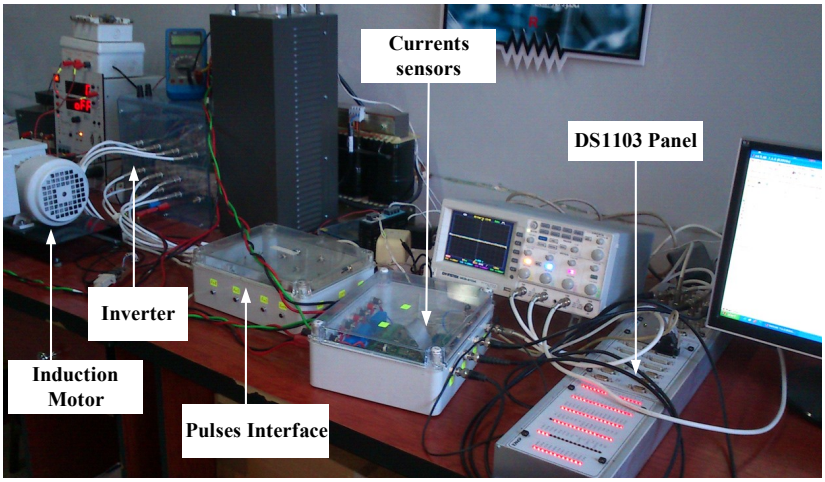

Figure 10. Experimental setup of FOC method

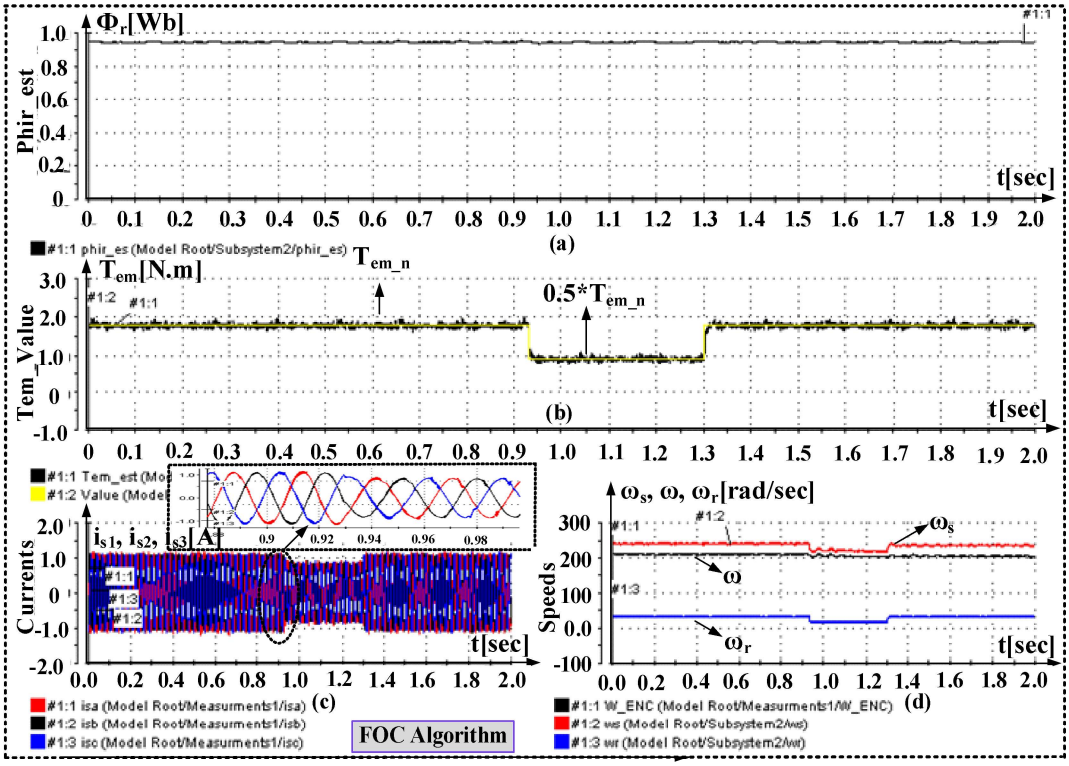

Figure 11. Experimental test of FOC strategy

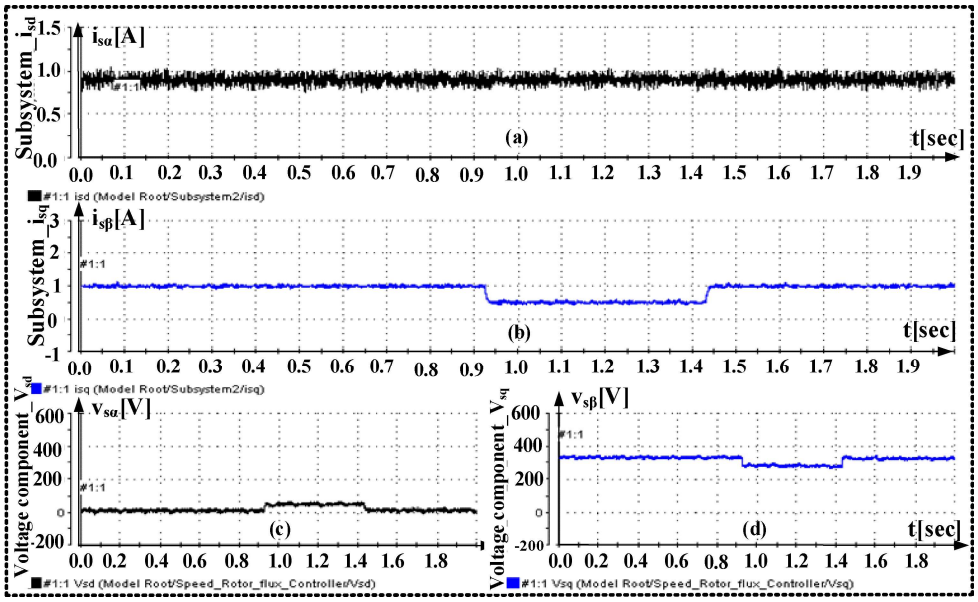

Figure 12. Experimental results of FOC: (a, b):The two components currents, (c,d): The two components voltatges

Celal Bayar University Journal of Science
Volume 20, Issue 3, 2024, p 47-57
Doi: 10.18466/cbayarfbe.1453798

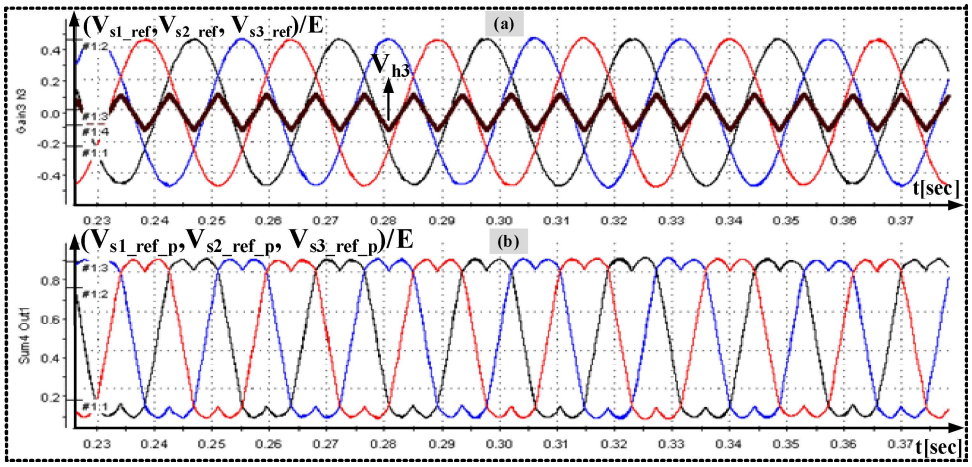

Figure 13. Reference voltages with the component of the third harmonic

The experiments were conducted so that they are largely compatible with the conditions of work at the simulation stage. The inverter frequency was set at 10 [KHz] and the sampling time was 50 [μs]. As shown in Figure (11), the nominal value of the rotor flux equalled 0.945[wb] was requested. Different torque reference values have been requested so that the performance of the algorithm with transient situations is ascertained. At the moment 0.9[sec], the nominal reference value of 1.76[N.m] was moved to half the nominal value. At the moment 1.3[sec] the nominal reference value of the torque was redialed again**.** It is noted that the rotor flux remained organized around the required reference value without any noticeable disturbances, and the generated torque well pursued the reference torque with high dynamics. The motor currents were sinusoidal ones without any jumps or turbulence, which confirmed that the performance has been quiet. It should be noted that the operation speed was about 210 [rad/sec], and the slip speed was variable between the nominal value and half the nominal value according to the torque value generated by the motor.

Figure (12) enhances the performance of the strategy, showing the components of stator current and voltage vectors in the synchronous reference frame. The value of the α-axis current component was 0.9[A], while the value of the β-axis component was changed between 1[A] and 0.5[A] depending on the torque range**.**

Figure (13) shows the reference three-phase voltage signals before being injected with the third harmonic signal divided by the DC-link (E) with the third grader signal. As mentioned above, an increase in the amplitude of the reference voltages can be secured by an increase of (15.47%), or reducing the DC-link by (15.47%).

6. Comparison with recent related papers

To verify the feasibility and effectiveness of the proposed algorithm, its performance is compared with previous and more recent approaches from the literature, specifically those in works referenced as [6, 9, 16]. As shown in Table (1), which presents seven works considered appropriate for comparison with the proposed control scheme, the algorithm's performance metrics are benchmarked against these established methods.

Table 1. Comparison with literature.

Used Method	**Proposed Method**	**Ref [6]**	**Ref [9]**	**Ref [16]**
Sample Time Type	Variable Step	Fixed Step	Fixed Step	Fixed Step
Antiwindup Technique	Yes	No	No	No
Third Harmonic Injection Technique	Yes	No	No	No
Optional Gains	4	4	6	6

Based on the table above, the benefits resulting from the proposed design, according to the characteristics outlined in the table, can be summarized as follows:

- **Variable Sampling Time**: The proposed algorithm offers high dynamics and accuracy when calculating state variables, unlike fixed-step-based methods, which may lack this accuracy.
- **Antiwindup Technique**: The proposed algorithm prevents PID regulators from exceeding permissible values. Without this feature, there's no guarantee that the regulator's outputs will stay within the allowed range.
- **Third Harmonic Injection Technique**: The proposed algorithm optimizes the DC-link voltage of the inverter, achieving a value that is 15.47% less than an algorithm without this property.
- **Optional Gains**: The small number of optional gains ensures simplicity in practical

implementation. Increased complexity occurs with a greater number of parameters. Therefore, the proposed strategy balances simplicity and effectiveness compared to other similar strategies..

7. Conclusions

In conclusion, the extensive laboratory testing of the proposed FOC algorithm on a well-equipped electric drive system test rig has empirically confirmed the robustness and effectiveness of the approach across a broad speed spectrum. The DS1103 digital processing card, central to the experimental platform, facilitated real-time control and monitoring, demonstrating the practical viability of transitioning from simulation to real-world application.

The experimental results have corroborated the simulated performance, with the inverter operating efficiently at a fixed frequency of 10 kHz and a precise sampling time of 50 µs. Notably, the system maintained the rotor flux at the nominal value of 0.945 wb without disturbances, even when faced with transient torque conditions. This stability is a testament to the algorithm's dynamic response capabilities, as the torque swiftly and accurately tracked the reference values.

Furthermore, the motor currents displayed an ideal sinusoidal waveform, indicative of the system's tranquility and absence of electrical noise. Operating at a speed of approximately 210 rad/sec, the system adeptly managed variations in slip speed, aligning with changes in the torque produced by the motor.

The strategic integration of stator current and voltage vectors, as illustrated in Figure (11), showcases the fine-tuned control achieved over the α and β components, further validating the precision of the system under variable torque demands.

Enhancements to the strategy are visually evident in Figure (12), where the implementation of third harmonic injection was found to notably increase the amplitude of reference voltages by 15.47%, concurrently allowing for a reduction in DC-link voltage requirements by the same margin.

These results not only validate the proposed FOC algorithm but also suggest potential for improvements in electric drive systems. With such clear demonstrations of enhanced performance and dynamic control, this research lays a strong foundation for future advancements, including potential integration with intelligent control systems, to further optimize performance and energy efficiency in varied and demanding industrial applications.

Acknowledgement

The authors declare that no acknowledgments are applicable for this study.

Author's Contributions

Mussaab Alshbib: was instrumental in conceptualizing the advanced FOC strategy, drafting and writing the manuscript, and performing the analytical analysis. contributed to enhancing the manuscript by providing insights into the practical applications of the FOC strategy, supervising the setup of the DS1103-controlled testbed, and ensuring the experimental verification aligned with real-world electric vehicle conditions. Both authors collaborated closely on all sections of the manuscript, ensuring a cohesive presentation of both the theoretical framework and experimental validation of the FOC strategy

Sohayb Abdulkerim: helped in performing the analytical analysis, performed the simulation work in MATLAB/Simulink, and result interpretation for the theoretical aspects of the study.S.A also played a key role in designing the experiment and analyzing experimental data to validate the simulation results.

Ethics

This study, which developed an advanced Field Oriented Control strategy for electric vehicle drivetrains, did not involve human or animal subjects and therefore did not require ethical approval. The work was purely analytical and simulation-based, adhering to relevant ethical standards for technical research. There are no ethical issues after the publication of this manuscript.

Conflict of Interest Statement:

The authors declare no potential conflicts of interest with respect to the research, authorship, and/or publication of this article. This includes, but is not limited to, financial, personal, or professional relationships that could be perceived to influence the work described in this manuscript.

References

[1]. M. Ganchev, "Control unit for a laboratory motor test bench for monitoring and controlling PMSM and induction motors," 2007 European Conference on Power Electronics and Applications, 2007, doi: 10.1109/epe.2007.4417431.

[2]. J. C. Nustes, D. P. Pau, and G. Gruosso, "Modelling the Field Oriented Control applied to a 3-phase Permanent Magnet Synchronous Motor," Software Impacts, vol. 15, p. 100479, Mar. 2023, doi: 10.1016/j.simpa.2023.100479.

[3]. R. Ghassani, Z. Kader, M. Fadel, P. Combes, and M. Koteich, "Comparison Study of Rotor Field-Oriented Control and Stator Field-Oriented Control in Permanent Magnet Synchronous Motors," 2023 IEEE International Electric Machines & Drives Conference (IEMDC), May 2023, doi: 10.1109/iemdc55163.2023.10239079.

[4]. Gudey, S.K.; Malla, M.; Jasthi, K.; Gampa, S.R. Direct Torque Control of an Induction Motor Using Fractional-Order Sliding Mode Control Technique for Quick Response and Reduced Torque Ripple. World Electr. Veh. J. 2023, 14, 137. https://doi.org/10.3390/wevj14060137

[5]. Alshbib, Mussaab M., Ibrahim Mohd Alsofyani, and Mohamed Mussa Elgbaily. 2023. "Enhancement and Performance Analysis for Modified 12 Sector-Based Direct Torque Control of AC Motors: Experimental Validation" Electronics 12, no. 3: 549. https://doi.org/10.3390/electronics12030549

[6]. B. Boomiraja and R. Kanagaraj, "DQ-axis Modelling and Field Oriented Control of Hybrid Flux Motor," Sep. 2022, doi: 10.21203/rs.3.rs-2008400/v1.

[7]. N. T. Dat, C. V. Kien, and H. P. H. Anh, "Optimal FOC-PID Parameters of BLDC Motor System Control Using Parallel PM-PSO Optimization Technique," International Journal of Computational Intelligence Systems, vol. 14, no. 1, p. 1142, 2021, doi: 10.2991/ijcis.d.210319.001.

[8]. Manepalli, Jaya Raju, and C. V. N. Raja. "Speed control of induction motor by ZN method and genetic algorithm optimization with PI and PID controller." Int J Innov Res Electr Electron Instrum Control Eng 3.3 (2015): 15-20.

[9]. S. -C. Chen and H. -K. Hoai, "Studying an Adaptive Fuzzy PID Controller for PMSM with FOC based on MATLAB Embedded Coder," 2019 IEEE International Conference on Consumer Electronics - Taiwan (ICCE-TW), Yilan, Taiwan, 2019, pp. 1-2, doi: 10.1109/ICCE-TW46550.2019.8991743.

[10]. V. S. Virkar and S. S. Karvekar, "Luenberger observer based sensorless speed control of induction motor with Fuzzy tuned PID controller," 2019 International Conference on Communication and Electronics Systems (ICCES), Coimbatore, India, 2019, pp. 503-508, doi: 10.1109/ICCES45898.2019.9002268.

[11]. A Mohammed Eltoum, M., Hussein, A. & Abido, M.A. Hybrid Fuzzy Fractional-Order PID-Based Speed Control for Brushless DC Motor. Arab J Sci Eng 46, 9423–9435 (2021). https://doi.org/10.1007/s13369-020-05262-3

[12]. J. Espina, A. Arias, J. Balcells and C. Ortega, "Speed Anti-Windup PI strategies review for Field Oriented Control of Permanent Magnet Synchronous Machines," 2009 Compatibility and Power Electronics, Badajoz, Spain, 2009, pp. 279-285, doi: 10.1109/CPE.2009.5156047.

[13]. H. P. H. Anh, C. V. Kien, T. T. Huan and P. Q. Khanh, "Advanced Speed Control of PMSM Motor Using Neural FOC Method," 2018 4th International Conference on Green Technology and Sustainable Development (GTSD), Ho Chi Minh City, Vietnam, 2018, pp. 696-701, doi: 10.1109/GTSD.2018.8595688.

[14]. A. A. Abdelrauf, W. W. Saad, A. Hebala and M. Galea, "Model Predictive Control Based PID Controller for PMSM for Propulsion Systems," 2018 IEEE International Conference on Electrical Systems for Aircraft, Railway, Ship Propulsion and Road Vehicles & International Transportation Electrification Conference (ESARS-ITEC), Nottingham, UK, 2018, pp. 1-7, doi: 10.1109/ESARS-ITEC.2018.8607585.

[15]. Uralde, J.; Barambones, O.; Artetxe, E.; Calvo, I.; del Rio, A. Model Predictive Control Design and Hardware in the Loop Validation for an Electric Vehicle Powertrain Based on Induction Motors. Electronics 2023, 12, 4516. https://doi.org/10.3390/electronics12214516.

[16]. Benbouhenni, H.; Bizon, N. Improved Rotor Flux and Torque Control Based on the Third-Order Sliding Mode Scheme Applied to the Asynchronous Generator for the Single-Rotor Wind Turbine. Mathematics 2021, 9, 2297. https://doi.org/10.3390/math9182297

[17]. L. Guo, D. Wang, Z. Peng, and L. Diao, "Improved super-twisting sliding mode control of a stand-alone DFIG-DC system with harmonic current suppression," IET Power Electronics, vol. 13, no. 7, pp. 1311–1320, May 2020, doi: 10.1049/iet-pel.2019.0691.

[18]. D. Zellouma, H. Benbouhenni, and Y. Bekakra, "Backstepping Control Based on a Third-order Sliding Mode Controller to Regulate the Torque and Flux of Asynchronous Motor Drive," Periodica Polytechnica Electrical Engineering and Computer Science, vol. 67, no. 1, pp. 10–20, Jan. 2023, doi: 10.3311/ppee.20333.

[**19].** R. S. Hiware and J. G. Chaudhari, "Indirect Field Oriented Control for Induction Motor," 2011 Fourth International Conference on Emerging Trends in Engineering & Technology, 2011, pp. 191-194, doi: 10.1109/ICETET.2011.56.

[20]. Kabache, Nadir.; Moulahoum, S.; Houassine, H" FPGA Implementation of direct Rotor Field Oriented Control for Induction Motor.

[21]. B. Bahrani, S. Kenzelmann and A. Rufer, "Multivariable-PI-Based dq Current Control of Voltage Source Converters With Superior Axis Decoupling Capability," in IEEE Transactions on Industrial Electronics, vol. 58, no. 7, pp. 3016-3026, July 2011, doi: 10.1109/TIE.2010.2070776.

[22]. G. Acevedo, Hernando, N. Vargas, G. M. Hernando, C. Torres and J. Jairo, "Design of Rotor Flux Oriented Vector Control Systems for Induction Motor," Proceedings of The 7th International Power Electronics and Motion Control Conference, 2012, pp. 1384-1388, doi: 10.1109/IPEMC.2012.6259010.

[23]. A. M. Trzynadlowski, "Dynamic model of the induction motor," Control of Induction Motors, pp. 107–117, 2001, doi: 10.1016/b978-012701510-1/50006-4.

[24]. G. Zhang, Z. Du, Yu. Ni, and C. Li, "Nonlinear model reduction-based induction motor aggregation," International Transactions on Electrical Energy Systems, vol. 26, no. 2, pp. 398–411, May 2015, doi: 10.1002/etep.2089.

[25]. H. Grotstollen and A. Bunte, "Control of induction motor with orientation on rotor flux or on stator flux in a very wide field weakening region-experimental results," Proceedings of IEEE International Symposium on Industrial Electronics, doi: 10.1109/isie.1996.551065.

[26]. H. Seo, G. Choe, J. Lim, and J. Jeong, "Slip frequency control of linear induction motor considering normal force in semi-high speed MAGLEV train," 2017 IEEE International Magnetics Conference (INTERMAG), Apr. 2017, doi: 10.1109/intmag.2017.8007999.

[27]. C. Zhou, Z. Cai, and F. Xie, "Research on speed regulation system of induction motor based on slip frequency control," 2018 13th IEEE Conference on Industrial Electronics and Applications (ICIEA), May 2018, doi: 10.1109/iciea.2018.8397926.

[28]. B. Singh, S. Pandey, A. Junghare and M. V. Aware, "Design of an anti-windup fractional order PI controller based on integral state predictor within stability bound," 2016 IEEE 1st International Conference on Power Electronics, Intelligent Control and Energy Systems (ICPEICES), Delhi, India, 2016, pp. 1-6, doi: 10.1109/ICPEICES.2016.7853493.

[29]. M. O. Ajangnay, "Optimal PID controller parameters for vector control of induction motors.," SPEEDAM 2010, Jun. 2010, doi: 10.1109/speedam.2010.5545043.

[30]. T. Singh, "Pole-Zero, Zero-Pole Canceling Input Shapers," Journal of Dynamic Systems, Measurement, and Control, vol. 134, no. 1, Dec. 2011, doi: 10.1115/1.4004576.

[31]. M. Ziyuan and Z. Xiaoqin, "Torque Calculation for A Nine-phase Induction Motor with Third-harmonic Current Injection," 2021 24th International Conference on Electrical Machines and Systems (ICEMS), Oct. 2021, doi: 10.23919/icems52562.2021.9634376.

[32]. M. Alshbib and S. Abdulkerim, "An Experimental and Analytical Investigation of the Direct Torque Control Method of a Three-Phase Induction Motor," Journal of Electrical Engineering & Technology, vol. 18, no. 6, pp. 4367–4379, Apr. 2023, doi: 10.1007/s42835-023-01483-2.

APPENDIX A

Calculation of the gains controllers for α and β loops:

The transfer function of the current control loop is as follows:

$$\frac{i_{s\alpha}}{i_{s\alpha\_ref}} = \frac{K_{P(\alpha)\_I}.b}{s + K_{P(\alpha)\_I}.b} \quad (1A)$$

The following equation is supposed:

$$a_5 = \frac{K_{I(\alpha)\_I}}{K_{P(\alpha)\_I}} \Rightarrow K_{I(\alpha)\_I} = a_5.K_{P(\alpha)\_I} \quad (2A)$$

The gain $K_{P(\alpha)\_I}$ is optional and can be set during the design.

The transfer function of the rotor flux is written as:

$$\frac{\Phi_r}{\Phi_{r\_ref}} = \frac{K_{P(\alpha)\_\Phi_r}.K_{P(\alpha)\_I}.b.a_2}{S^2 + K_{P(\alpha)\_I}.b.S + K_{P(\alpha)\_\Phi_r}.K_{P(\alpha)\_I}.b.a_2} \quad (3A)$$

The following equation is supposed:

$$a_1 = \frac{K_{I(\alpha)\_\Phi_r}}{K_{P(\alpha)\_\Phi_r}} \quad (4A)$$

One can suppose that $\xi = \frac{1}{\sqrt{2}}$),

$$\left.\begin{aligned} 2\zeta\omega_n = K_{P(\alpha)\_I}.b \Rightarrow \omega_n = \frac{K_{P(\alpha)\_I}.b}{2.\frac{1}{\sqrt{2}}} \\ \omega_n{}^2 = K_{P(\alpha)\_\Phi_r}.K_{P(\alpha)\_I}.b.a_2 \end{aligned}\right\} \Rightarrow K_{P(\alpha)\_\Phi_r} = \frac{\omega_n{}^2}{K_{P(\alpha)\_I} b\, a_2} \quad (5A)$$

$$K_{I(\alpha)\_\Phi_r} = a_1.K_{P(\alpha)\_\Phi_r} \quad (6A)$$

$$\frac{i_{s\beta}}{i_{s\beta\_ref}} = \frac{K_{P(\beta)\_I}.b}{S + K_{P(\beta)\_I}.b} \quad (7A)$$

Where the following equation was supposed:

$$a_5 = \frac{K_{I(\beta)\_I}}{K_{P(\beta)\_I}} \Rightarrow K_{I(\beta)\_I} = a_5.K_{P(\beta)\_I} \quad (8A)$$

The value of $K_{P(\beta)\_I}$ is optional and can be set during the design.

For the Speed loop gains, they can be obtained through the following equations:

$$\frac{\omega}{\omega_i} = \frac{\frac{K_p K_{P\_I} b P^2 L_m \Phi_{r\alpha}}{JL_r}}{S^2 + K_{P\_I} bS + \frac{K_p K_{P\_I} b P^2 L_m \Phi_{r\alpha}}{JL_r}} \quad (9A)$$

The propotional gain K_v can be calculated (suppose that $\xi = 1$) as follows,

$$K_V = \frac{JL_r \omega_{n1}^2}{K_{P\_I} b P^2 L_m \Phi_{r\alpha}} \quad (10A)$$

Where:

$$\omega_{n1}^2 = \frac{K_{P\_I} b}{2} \quad (11A)$$

The final transfer function can be written as

$$\frac{\omega}{\omega_{ref}} = \frac{\frac{K_{p\_\omega} K_p K_{P\_I} b P^2 L_m \Phi_{r\alpha}}{JL_r}}{S^2 + \omega_{n1} S + \frac{K_{p\_\omega} K_p K_{P\_I} b P^2 L_m \Phi_{r\alpha}}{JL_r}} \quad (12A)$$

So one can get

$$K_{p\_\omega} = \frac{\omega_n{}^2 JL_r}{K_p K_{P\_I} b P^2 L_m \Phi_{r\alpha}} \quad (13A)$$

APPENDIX B: The used motor parameters

Nominal voltage	230/400[V]
Phase resestance stator	R_s=45.83[Ω]
Phase resestance rotor	R_r=31[Ω]
Phase inductance stator	L_s=1.24[H]
Phase inductance rotor	L_r=1.11[H]
Mutual inductance	L_m=1.05[H]
Inertia	$J = 0.006$ [kg.m^2]
Friction factor	f=0.001[N.m.sec/rad]
Number of poles pairs	p=2
Nominal stator flux	Φ_s=1.14[H]
Nominal power	P_n=0.25[kW]
Nominal frequency	F=50[Hz]
Nominal speed	N=1350[rpm]
Nominal torque	T_{em}=1.76[N.m]
Slip speed	ω_r=29.5[r/s]